



Modeling and simulation of high speed sliding

Zhigang Wei^{a,*}, R.C. Batra^{b,1}

^a Department of Aerospace Engineering and Engineering Mechanics, The University of Texas at Austin, Austin, TX 78712, USA

^b Department of Engineering Science and Mechanics, Mail Code 0219, Virginia Polytechnic Institute and State University, Blacksburg, VA 24061, USA

ARTICLE INFO

Article history:

Received 26 March 2009

Received in revised form

8 June 2010

Accepted 11 June 2010

Available online 18 June 2010

Keywords:

Contact melting

Deformation localization

Plastic dissipation

High speed sliding

Melt lubrication

ABSTRACT

We analyze the processes of thermal softening, melting and subsequent melt lubrication that occur during the high speed sliding of a metal piece on another metal block. The temperature rise in the slider arising from both high speed interface friction and from the energy dissipated during plastic deformations is computed using simple analysis and the finite element method. Subsequently, we propose a mathematical model for the transient lubrication problem that describes the behavior of the molten film at the slider–rail interface. This model successfully predicts the evolution process of the melt thickness and the melt front velocity of the liquid film; these predictions agree with the experimentally observed dynamics of molten film better than those from other existing models.

© 2010 Elsevier Ltd. All rights reserved.

1. Introduction

Contact melting is a basic phase change phenomenon occurring at the interface between two solid bodies sliding past each other at a high speed when one of them is heated above its melting temperature due to either external heat sources or internal mechanisms such as viscous heating [1]. Recently, Bejan has presented a comprehensive review of different aspects of contact melting [2,3]. Contact melting due to high speed sliding plays a significant role in diverse applications such as water film formation in ice during sled sliding [4], the interior ballistics associated with the melting band of a projectile traveling along a gun barrel [5,6], and the molten film formation in armature–rail surface [7–9].

Thermal softening and melting during high speed solid metal/metal friction resulting in melt lubrication are some of the phenomena that accompany contact-melting processes. Modeling the physics of high speed metal/metal friction can be very challenging since coupled thermal, mechanical [10] and sometimes chemical reactions are involved in this process [11]. Not surprisingly, the melting process and the subsequent melt lubrication have been treated separately by researchers working in solid and fluid

mechanics. While melting and lubrication are indeed two distinct processes in contact-melting problems, in many applications the solution of one is required before the other can be studied. For example, as we demonstrate in this paper, analyzing unsteady lubrication requires that the emergent time of melting be provided as an initial condition. Here we study the physics of melting and lubrication in a contact-melting process in a unified manner. Said explicitly, we attempt to answer the following question: how does a solid slider soften and eventually melt during the sliding process? We consider different sliding mechanisms and account for two different contributions to the melting of the slider material, and model the softening and melting of a solid at high speed of sliding.

The second part of the paper focuses on studying the lubrication following the onset of melting. In most investigations reported in the literature [1–4,6,8,9], the contact-melting process has been considered quasi-steady; thus those works are unable to accurately predict the transient phenomena observed in experimental systems such as armature–rail sliding [12]. Here a mathematical model for the transient problem is developed and provides a more realistic interpretation of experimental results. A similar approach has been proposed by Yoo [13,14] to investigate the transient behavior in early stages of gravity-induced contact melting.

This paper is organized as follows. In Section 2, we develop a simple model using the parabolic heat equation to obtain a quantitative dependence of the melting time and the distance traveled by the slider upon the slider speed, material properties, and the pressure acting on the slider. The finite element method

* Corresponding author. Present address: 3-1-07C, 505 King Ave., Columbus, OH 43201, USA. Tel.: +1 614 424 6477.

E-mail addresses: weiz@battelle.org (Z. Wei), rbatra@vt.edu (R.C. Batra).

¹ Tel.: +1 540 231 6051.

Nomenclature	
<i>Dimensional variables</i>	
\bar{A}	yield strength, Pa
a	acceleration, m/s^2
\bar{B}	strain hardening strength, Pa
c	specific heat, $J/(kg K)$
C	strain-rate hardening coefficient
D	distance the slider traveled, m
f	friction coefficient
F_n	normal force per unit length, N/m
F_f	frictional force per unit length, N/m
G	pressure gradient, N/m^3
h_{sf}	latent heat, J/kg
H	specimen thickness, m
k	thermal conductivity, $W/(m K)$
L	slider length, m
N	element number
n	exponent shown in Eq. (9)
P	pressure, Pa
q	heat flux, W/m^2
Q	flow rate, m^2/s
R	constant in Eq. (15)
t	time, s
T_m, T_0	melting and reference temperature, K
U	velocity of slider, m/s
U_{slip}	slip velocity, m/s
U_t	shearing velocity, m/s
V	Melt front velocity, m/s
u, v	velocity components along x, y directions, m/s
x, y	Cartesian coordinates
<i>Greek symbols</i>	
$\alpha = k/\rho c$	thermal diffusivity, m^2/s
β	partitioning of energy
ρ	density, kg/m^3
δ	liquid film thickness, m
γ	strain
$\dot{\gamma}$	strain rate
τ	shear stress
δ_d, δ_T	thickness of boundary layer
ξ	integral variable, s
μ	shear modulus, Pa
<i>Subscripts</i>	
c	a critical state at which steady state is achieved
r	rail
s	slider
S	steady state
<i>Definitions of non-dimensional variables</i>	
y	\bar{y}/H
t	$\bar{t}\dot{\gamma}_0$
θ	$\bar{\theta}\bar{\rho}\bar{c}/\tau_0$
k	$\bar{k}/\bar{\rho}\bar{c}\dot{\gamma}_0 H^2$
ρ	$\bar{\rho}H^2\dot{\gamma}_0^2/\tau_0$
q	$\bar{q}/\dot{\gamma}_0 H\tau_0$
η	y/δ
f	F_t/F_n
\bar{t}	$t\alpha/L^2$
\bar{V}	VL/α
\bar{U}	UL/α
$\bar{\delta}$	δ/L
\hat{V}	\bar{V}/\bar{V}_S
\hat{t}	$\bar{t}\bar{V}_S/\bar{\delta}_S$
$\hat{\delta}$	$\bar{\delta}/\bar{\delta}_S$
B_e	$F_n L/\mu\alpha$
S_{te}	$c(T_m - T_0)/h_{sf}$
$S_{te\mu}$	$c\mu U^2/kh_{sf}$
W	$c\mu\alpha^2/L^2 kh_{sf}(1 + S_{te})$

(FEM) is subsequently used to find an approximate solution of coupled thermo-mechanical equations which predicts the formation of the localization layer followed by melting of the material. In Section 3, equations governing the transient contact melting are derived with adiabatic thermal condition imposed at the interface near the rail surface and theoretical predictions are compared with experimental results. Conclusions of this work are summarized in Section 4.

2. Modeling thermal softening and melting at slider surface

As shown schematically in Fig. 1, a slider is pushed with a constant pressure P against a rail and moves to the right with (in general, a time dependent) velocity $U(t)$. Similar configurations have served as models for studying simple shear [15,16], pressure-shear [10], and other sliding systems [4,6,8,9]. During sliding the contact between the slider and the rail is initially solid/solid as shown in Fig. 1(a). The tangential force due to interface friction acts on both the slider and the rail and raises their temperatures. If a shear-induced plastic deformation is also involved in the sliding process, then plastic dissipation will also contribute to the temperature rise. During high speed sliding, the temperature rise due to these contributions can become very high, leading to melting of the slider [10–12] material. After melting, the thickness $\delta(t)$ of the molten film increases with time and approaches a steady

state value sustained by the balance between the heat generated due to viscous dissipation and that lost via heat conduction, and the slider moves downward with velocity $V(t)$ due to the imposed pressure, as shown in Fig. 1(b).

2.1. Heat generation and temperature rise due to interface friction

In this subsection, we analytically analyze the initiation of the melting process due to the interface friction. Subsequently, we will consider the effects of plastic dissipation and numerically solve the problem.

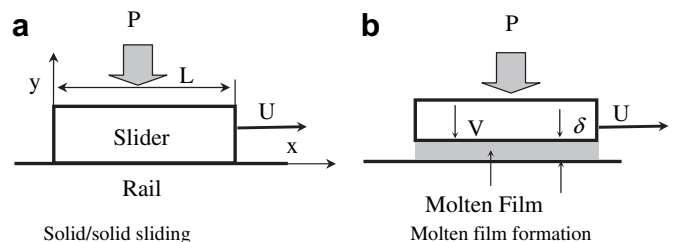


Fig. 1. Schematics of solid/solid sliding. (a) Solid/solid sliding (b) molten film formation.

The calculation of the temperature rise in the slider requires an estimate of the heat generated when the slider moves over the rail. Assuming that all of the mechanical working is converted into heating the slider and the rail, the heat flux q generated at the metal/metal interface can be written as

$$\begin{aligned} q &= \beta \tau U_{\text{slip}} \\ \tau &= fP \end{aligned} \tag{1}$$

where τ, f, P and U_{slip} are the shear stress, the coefficient of friction, the normal pressure between the slider and the rail, and the slip velocity, respectively. The constant β quantifies the partitioning of the heat flux between the slider and the rail. Its value found by equating the temperatures in the rail and the slider at the slider–rail interface (and the total heat flux to q) is given by (e.g. see Carslaw and Jaeger [17])

$$\beta = \frac{k_s \sqrt{\alpha_r}}{k_s \sqrt{\alpha_r} + k_r \sqrt{\alpha_s}} \tag{2}$$

Here k and α are the thermal conductivities and the thermal diffusivities, with subscripts s and r representing, respectively, the slider and the rail. For an aluminum slider on a copper rail, $\beta \sim 0.29$, i.e., about 29% of the heat generated at the interface due to frictional effects is transferred to the aluminum slider and nearly 71% into the copper rail. Using representative experimental data [12], $P \sim 10^7 - 10^8$ MPa, $U_{\text{slip}} \sim 10^2 - 10^3$ m/s, $\beta f \sim 10^{-2} - 10^{-1}$, the typical value of the heat flux is estimated to be $q = 10^7 - 10^{10}$ W/m².

Here we assume that the interfacial slip velocity (and hence heat flux) is known, and compute the temperature rise in the slider as a function of time and the distance from the slider–rail interface using a one-dimensional transient heat conduction equation with pertinent initial and boundary conditions. The temperature rise in the rail can also be computed by solving the corresponding initial boundary value problem, but is not of interest here. This analysis gives the temperature at the slider–rail interface, which is used to estimate the time elapsed (and hence the distance traveled by the slider) before the onset of melting.

For a time-dependent heat flux $q(t)$ arising from a time-dependent slider velocity, the temperature rise from the initial uniform temperature can be approximated by [17]

$$T = \frac{1}{k} \sqrt{\frac{\alpha}{\pi}} \int_0^t q(t - \xi) e^{-\frac{y^2}{4\alpha\xi}} \frac{d\xi}{\tau^{1/2}} \tag{3}$$

At the interface $y = 0$ we have

$$T|_{y=0} = \frac{1}{k} \sqrt{\frac{\alpha}{\pi}} \int_0^t q(t - \xi) \frac{d\xi}{\tau^{1/2}} \tag{4}$$

In many applications, the slider velocity can be approximated by the power law [18]

$$U = at^n \tag{5}$$

where a and n are constants. For n not equal to -1 , the distance D traveled by the slider in time t and obtained by integrating Eq. (5) is given by $D = at^{n+1}/(n+1)$. Two special cases are of interest: first, when $n = 0$, $U = a$ and $D = at$; and second, when $n = 1$, $U = at$, $D = at^2/2$, the acceleration is constant.

For constant velocity (and hence constant heat flux q) we have,

$$T|_{y=0} = \frac{2q}{k} \sqrt{\frac{\alpha t}{\pi}} \tag{6}$$

Combining Eqs. (1) and (6) and setting $T|_{y=0} = T_{m0} = T_m - T_0$, we can find the time t_m when the slider surface touching the rail melts, and the corresponding distance traveled by the slider D_m :

$$t_m = \frac{\pi}{\alpha} \left(\frac{kT_{m0}}{2\beta f P U_{\text{slip}}} \right)^2 \tag{7}$$

$$D_m = U_{\text{slip}} t_m = \frac{\pi}{\alpha U_{\text{slip}}} \left(\frac{kT_{m0}}{2\beta f P} \right)^2 \tag{8}$$

Assuming that the experimental data reported in Ref. [12] is representative of such problems, we can derive general trends of t_m, D_m dependence upon the pressure P . For $P = 45$ MPa, $U_{\text{slip}} = 800$ m/s, $D_m = 0.6$ m we obtain $t_m = 0.751$ s, and $f = 0.0286$. Using $f = 0.0286$, the predicted values of t_m, D_m for other values of P are listed in Table 1. The general trend we observe is that both t_m, D_m decrease with an increase in the pressure P .

The experimentally observed sliding speed reported in Ref. [12] can be approximated as a linear function of time, i.e., by taking $n = 1$ in Eq. (5), with the constant acceleration a of 10^6 m/s². Then combining Eqs. (1), (4) and (5) we obtain

$$T|_{y=0} = \frac{4\beta f P a}{3k} \sqrt{\frac{\alpha}{\pi}} t^{\frac{3}{2}} \tag{9}$$

and

$$t_m = \left(\frac{\pi}{\alpha} \right)^{\frac{1}{3}} \left(\frac{3kT_{m0}}{4\beta f P a} \right)^{\frac{2}{3}} \tag{10}$$

$$D_m = \frac{1}{2} a t_m^2 = \frac{1}{2a^{1/3}} \left(\frac{\pi}{\alpha} \right)^{\frac{2}{3}} \left(\frac{3kT_{m0}}{4\beta f P a} \right)^{\frac{4}{3}} \tag{11}$$

For $P = 45$ MPa, $U_{\text{slip}} = 800$ m/s, $D_m = 0.6$ m, we get $t_m = 1.095$ s and $f = 0.0259$. Using $f = 0.0259$, the computed values of t_m, D_m for other values of the pressure, P , are listed in Table 1. The general trends of the dependence of t_m, D_m upon the pressure are the same as those for the constant velocity case. However, values of t_m, D_m for the constant acceleration case are larger than those when the velocity is constant. This is reasonable since less energy is generated during early stages when the armature speed varies linearly with time.

2.2. Heating due to coupled interface friction and plastic dissipation

The physics of motion of a slider over a rail is more involved than that described above in the simple interfacial friction model [11]. A characteristic of high speed sliding is that the friction induced localized deformations can occur at the interface [10,11]. We note that deformations of the slider are shear dominated with a significant heat flux at the boundaries. Accordingly, we study the simple shearing deformations of a thermo-elasto-viscoplastic material with both the tangential velocity and the heat flux prescribed at the boundaries, and delineate the localization of deformation in the region adjoining the boundaries. Recently, Batra and Wei [15] investigated a similar problem by using the FEM, and found that

Table 1

Predicted melting time and the corresponding distance traveled for constant velocity and constant acceleration.

P (MPa)	Constant velocity		Constant acceleration	
	t_m (ms)	D_m (m)	t_m (ms)	D_m (m)
45	0.751	0.6	1.095	0.6
75	0.270	0.216	0.780	0.304
89	0.192	0.154	0.696	0.242
117	0.111	0.089	0.580	0.168
150	0.018	0.054	0.491	0.121

the prescribed constant heat flux made deformations inhomogeneous and introduced a nucleation site for the deformations to localize. However, the manner in which the prescribed heat flux affects the temperature rise (and hence melting) was not addressed. Additionally, the width of the localized region was not computed in Ref. [15]; these issues are addressed below.

2.2.1. Formulation of the problem

We study simple shearing deformations of a homogeneous and isotropic thermo-elasto-viscoplastic body occupying the domain $0 \leq y \leq H$, and sheared by tangential velocity U_t with the heat flux q prescribed on the surface $y=0$. Thus both mechanical and thermal energies are input into the body through the boundary. The relation between the slip velocity U_{slip} , the tangential velocity U_t , and the velocity U of a slider is $U_{\text{slip}} + U_t = U$. Let the spatial coordinate be normalized by H , the shear stress by τ_0 , time by H/U_t , and the temperature by T_0 . In terms of non-dimensional variables, the body occupies the domain $0 \leq y \leq 1$.

The governing equations, as well as the initial and the boundary conditions are listed below.

$$\begin{aligned} \rho \frac{\partial v}{\partial t} &= \frac{\partial \tau}{\partial y}, \quad \rho C \frac{\partial T}{\partial t} = k \frac{\partial^2 T}{\partial y^2} + \tau \dot{\gamma}_p, \quad \dot{\gamma} = \frac{\partial v}{\partial y}, \quad \dot{\gamma} = \dot{\gamma}_e + \dot{\gamma}_p \\ \dot{\tau} &= \mu \dot{\gamma}_e, \quad \dot{\gamma}_p = \dot{\gamma}_0 \exp \left[\left(\frac{\tau}{(A+B\dot{\gamma}^n)(1-T^m)} - 1 \right) / C \right], \quad T_* = \frac{T-T_0}{T_m-T_0} \end{aligned} \quad (12)$$

In Eqs. (12) a superimposed dot indicates the material time derivative, ρ is the mass density, v the velocity, τ the shear stress, γ the shear strain, $\dot{\gamma}$ the shear strain rate, t the time, and T the present temperature of a material particle. Furthermore, k is the thermal conductivity, and μ the shear modulus of the material of the slider. Eqs. (12)₁ and (12)₂ express, respectively, the balance of linear momentum, and the balance of internal energy. All of plastic working, given by the second term on the right-hand-side of Eq. (12)₂, is assumed to be converted into heating. Eq. (12)₃ is the definition of strain rate, and Eq. (12)₄ implies that the strain rate is composed of elastic and plastic parts. Eq. (12)₅ is Hooke's law written in the rate form, and Eq. (12)₆ is the Johnson and Cook [19] thermo-viscoplastic relation. In it $\dot{\gamma}_0$ is the reference strain rate, and T_m and T_0 are the fictitious melting temperature and the reference temperature, respectively; T_m is a curve fitting parameter rather than the actual melting temperature of the material. Parameters m , n and C characterize, respectively, the thermal softening, strain hardening, and strain-rate hardening of the material. All material parameters are presumed to be constants for the range of strains, strain rates and temperatures anticipated to occur in the problem. Table 2 lists values of material parameters taken from Batra and Kim [16] for the 7039 aluminum; some of these values are a little different from those used in the preceding analysis. We note that the empirical Johnson–Cook relation was derived from test data over a limited range of strains, strain-rates, and temperatures that is considerably less than that anticipated to occur within a localized zone. Also, for some materials, phase transitions, damage, and melting may occur in the severely deformed region; these are not considered in Eqs. (12). Thus, results presented herein are approximate, give orders of magnitude of different variables, and help establish general trends.

Table 2
Material parameters used in the Johnson–Cook relation for 7039 Aluminum.

$\bar{\rho}$, kg/m ³	\bar{c} , J/kg °C	$\bar{\mu}$, GPa	\bar{k} , W/m °C	T_m , °C	τ_0 , MPa	\bar{A} , MPa	\bar{B} , MPa	C	n	m
2770	875	28	149	604	193	193	157	0.01	0.41	1.0

For initial conditions, we assume

$$\tau(y, 0) = \tau_0, \quad \gamma(y, 0) = \gamma_0 \approx 0, \quad \dot{\gamma}(y, 0) = \dot{\gamma}, \quad T(y, 0) = 0,$$

For boundary conditions we take

$$\begin{aligned} -k \partial T / \partial y(0, t) &= q(t), \quad -k \partial T / \partial y(H, t) = 0, \\ v(0, t) &= U_t, \quad v(H, t) = 0 \end{aligned}$$

The non-dimensional parameters are related to their dimensional (barred) counterparts as follows:

$$\begin{aligned} y &= \bar{y}/H, \quad t = \bar{t} \dot{\gamma}_0, \quad \theta = \bar{\theta} \bar{\rho} \bar{c} / \tau_0, \quad k = \bar{k} / \bar{\rho} \bar{c} \dot{\gamma}_0 H^2, \\ \rho &= \bar{\rho} H^2 \dot{\gamma}_0^2 / \tau_0, \quad q = \bar{q} / \dot{\gamma}_0 H \tau_0. \end{aligned} \quad (13)$$

2.2.2. Computation and discussion of results

In order to compute results, we set $H=3$ mm, $U_t=3, 15, 30, 150$, and 300 m/s. Hence, the block is sheared at a nominal strain-rate of $10^3, 5 \times 10^3, 10^4, 5 \times 10^4, 10^5$ /s. For $\alpha = 10^{-5}$ m²/s, $t = 10^{-4} - 10^{-3}$ s, the thermal diffusion length $L_d = 2\sqrt{\alpha t}$ is of the order of 10^{-1} mm, and the slab is sufficiently thick to be considered as semi-infinite. The afore-stated problem is solved numerically by the FEM, and the coupled nonlinear ordinary differential equations are integrated with respect to time by using the subroutine LSODE with $MF=22$, $ATOL=10^{-7}$, and $RTOL=10^{-7}$. Parameters $ATOL$ and $RTOL$ control, respectively, the absolute and the relative tolerances in the solution. The FE code [16] has been modified to incorporate the non-zero heat flux boundary condition at $y=0$, and its verification is described in [15]. We used two FE meshes – one with coordinates of nodes given by

$$\begin{aligned} y_n &= 1 - \left[R + \frac{(n-1)}{N} \right]^{0.4}, \quad 1 \leq n \leq 100 \\ y_n &= 1 - \frac{1}{6} \left[5 + \frac{(n-101)}{(N-100)} \right], \quad n \geq 101 \end{aligned} \quad (14)$$

where $R=1.9, 2.51$, and 3.14 , respectively, for $N=300, 400$, and 500 , and the other with nodal coordinates given by

$$\begin{aligned} y_n &= 1 - \left[8 \left(\frac{n-1}{300} \right) \right]^{0.6}, \quad 1 \leq n \leq 31; \\ y_n &= 1 - \left(\frac{n-1}{300} \right)^{0.05}, \quad 31 \leq n \leq 301. \end{aligned}$$

These two FE meshes gave virtually identical results, and the results presented below are with the mesh described by Eq. (14) and $N=400$; the length of each one of the 400 elements close to the surface $y=0$ is $1.25 \mu\text{m}$.

For the nominal strain rate of 10^4 s^{-1} and seven values of the heat flux prescribed at $y=0$, time histories of evolution at $y=0$ of (a) the non-dimensional temperature rise, and (b) the non-dimensional shear stress are plotted in Fig. 2(a), (b). It can be seen that the initial rate of temperature increase varies with the prescribed heat flux, followed by an “explosive” increase in temperature, the occurrence of which is essentially independent of the prescribed heat flux. However, the time when the steep temperature rise occurs decreases rapidly with an increase in the prescribed heat flux. The rapid temperature increase shown in

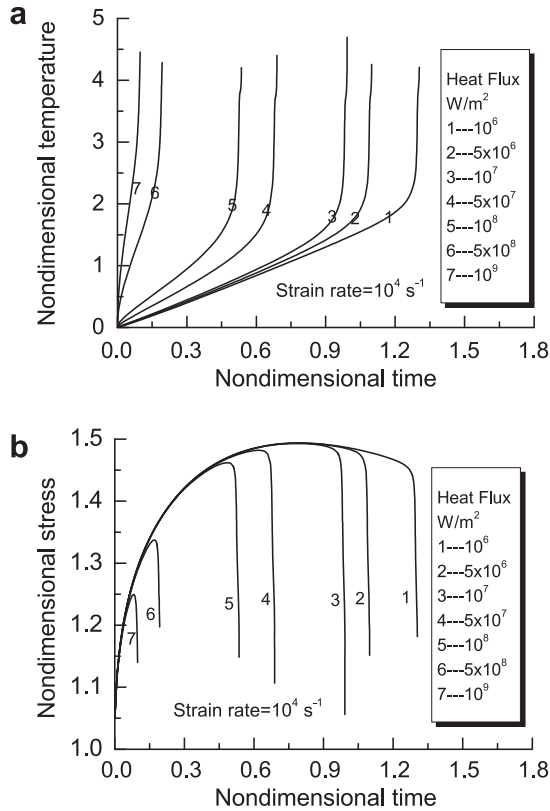


Fig. 2. For seven values of the heat flux prescribed at $y = 0$, time histories at $y = 0$ of (a) the non-dimensional temperature rise, and (b) the non-dimensional shear stress.

Fig. 2(a) is directly related to the dramatic drop in the shear stress shown in Fig. 2(b) and indeed both are seen to occur concurrently.

Fig. 3 depicts, for heat flux of 10^8 W/m^2 prescribed at $y = 0$, and a nominal strain rate of 10^4 s^{-1} , the spatial distribution of (a) the non-dimensional shear stress, (b) the non-dimensional temperature, and (c) the shear strain at different times. It is clear that for $t = 0.11, 0.25$ and 0.49 , the shear stress and the shear strain are uniform over the specimen, with the shear stress gradually increasing till it peaks. However, the temperature distribution is non-uniform at all times with the highest temperature occurring at $y = 0$ and the lowest at $y = 1$. Because of the continuing rise in temperature difference between the material point at $y = 0$ and those at $y > 0$ the deformations are inhomogeneous, and the shear stress at $y = 0$ peaks first and subsequently drops rapidly as indicated by curves 4 and 5 in Fig. 3(a).

The narrow region of intense plastic deformation and temperature increase near the surface $y = 0$ is usually called a shear band. We note that Cho et al.'s [20] micro-hardness measurements across an intensely deformed region in a HY-100 steel reveal two characteristic length scales: a well-defined band width of $20 \mu\text{m}$ (deformation localization) surrounded by a $100 \mu\text{m}$ wide heat diffusion length called the heat affected zone (HAZ, or thermal localization). If δ_d denotes the thickness of the region over which strain γ varies rapidly from $\gamma(y)$ to $\gamma(0)$ and δ_T the thickness of the region in which T varies dramatically from $T(y)$ to $T(0)$ we define δ_d and δ_T as the locations at which $[\gamma(0) - \gamma(y)]/[\gamma(0) - \gamma(1)] = [T(0) - T(y)]/[T(0) - T(1)] = \lambda$, where λ is a scaling factor, and $0 < \lambda < 1$. We refer to δ_d and δ_T as the deformation boundary layer thickness and the thermal boundary layer thickness, respectively. Both δ_d and δ_T can be found by measuring strain and temperature profiles in space at a certain time, at which the stress ratio τ/τ_{max} at $y = 0$ has dropped to

a preassigned value. This definition, like others used heretofore, is somewhat arbitrary and not unique, but we use it to help establish general trends; e.g. also see Ref. [24].

For our system, at different values of τ/τ_{max} at the point $y = 0$, Fig. 4 depicts the dependence of δ_d and δ_T upon the ratio τ/τ_{max} and the parameter λ . Increasing λ and τ/τ_{max} is seen to increase both δ_d and δ_T . Moreover, δ_d is generally less than δ_T for the same values of τ/τ_{max} and λ , which agrees with the experimental observation that the width of the well-defined deformation band is smaller than that of HAZ. For example, for $\lambda = 0.5$ and $\tau/\tau_{\text{max}} = 0.95$, we obtain $\delta_T = 25 \mu\text{m}$, $\delta_d = 14 \mu\text{m}$. These values of the boundary layer thickness compare well with the experimentally observed thickness of molten aluminum deposited on copper rail of less than $25 \mu\text{m}$ by Persad et al. [7]. We note that values of material parameters for the aluminum used by Persad et al. [7] may be different from those employed here; nevertheless, the closeness of the magnitude of the thickness of the molten film to that of the localized region is very encouraging. It suggests that the molten film is formed from a localized deformation layer.

2.2.3. Contributions to heating from interface friction and plastic dissipation

As shown in the preceding sections, the heat flux due to interface friction and plastic dissipation can melt the material. However, the relative importance of the plastic working and the interface heating in a coupled thermo-mechanical system is unknown. In order to clarify this, we assume that the deformations of the slider near the interface are uniform and occur at a constant strain rate and at a constant stress level. The estimated temperature rise due to plastic dissipation is then given by $T = \tau \dot{\gamma} t / \rho c$ where we have assumed that the plastic strain rate equals the total strain rate. Setting the temperature rise equal to that given by Eq. (6) we get $q = \tau \dot{\gamma} \sqrt{\alpha t} / 2$. For typical values of parameters like $\tau \sim 200 \text{ MPa}$, $t \sim 10^{-4} \text{ s}$, $\dot{\gamma} \sim 10^4 \text{ s}^{-1}$, we obtain $q \sim 10^8 \text{ W/m}^2$. Thus the contribution of the heat flux at the interface to the temperature rise can be neglected when $q \leq 10^8 \text{ W/m}^2$, and the heat flux will play equal or even more prominent role than plastic dissipation when $q > 10^8 \text{ W/m}^2$.

The actual situation is, however, more complex than that described above since the deformation is far from being uniform at points near the interface and is also time dependent. For $q = 10^8 \text{ W/m}^2$ and $q = 10^{10} \text{ W/m}^2$, respectively, Fig. 5(a), (b) depicts the temperature rise at $y = 0$ due to the interface heating only, and the combined effects of the interface heating and the plastic dissipation in a specimen deformed at a nominal strain rate 10^4 s^{-1} obtained by solving the governing equations by the FEM. For $q = 10^8 \text{ W/m}^2$ and for small values of time, the contributions from the two sources are found to be comparable, and agree with the result predicted by our simple analysis. For example, the interface heating induced temperature rise is 32.5 K at time 0.03 ms while the total temperature rise is 75.4 K . Thus, almost one-half of the temperature rise is due to the interface heating. However, the plastic dissipation makes a more dominant contribution to the temperature rise in the late stage of sliding, e.g., the temperature rise due to the interface friction heating is 44.1 K at time 0.054 ms while the total temperature rise is more than 334.6 K . Hence only about $1/8$ th of the total temperature rise comes from the interface heating. The rapid rise in temperature and the concave shape of the temperature rise vs. time curve are intrinsic characteristics of the deformation localized into a thin layer. For $q = 10^{10} \text{ W/m}^2$, the temperature rise is controlled by the interface heating at all times, e.g., at low temperature the two curves cannot be distinguished from each other implying that the temperature rise is almost totally due to the interface heating. With the passage of time, the plastic dissipation begins to contribute to the temperature rise, but still

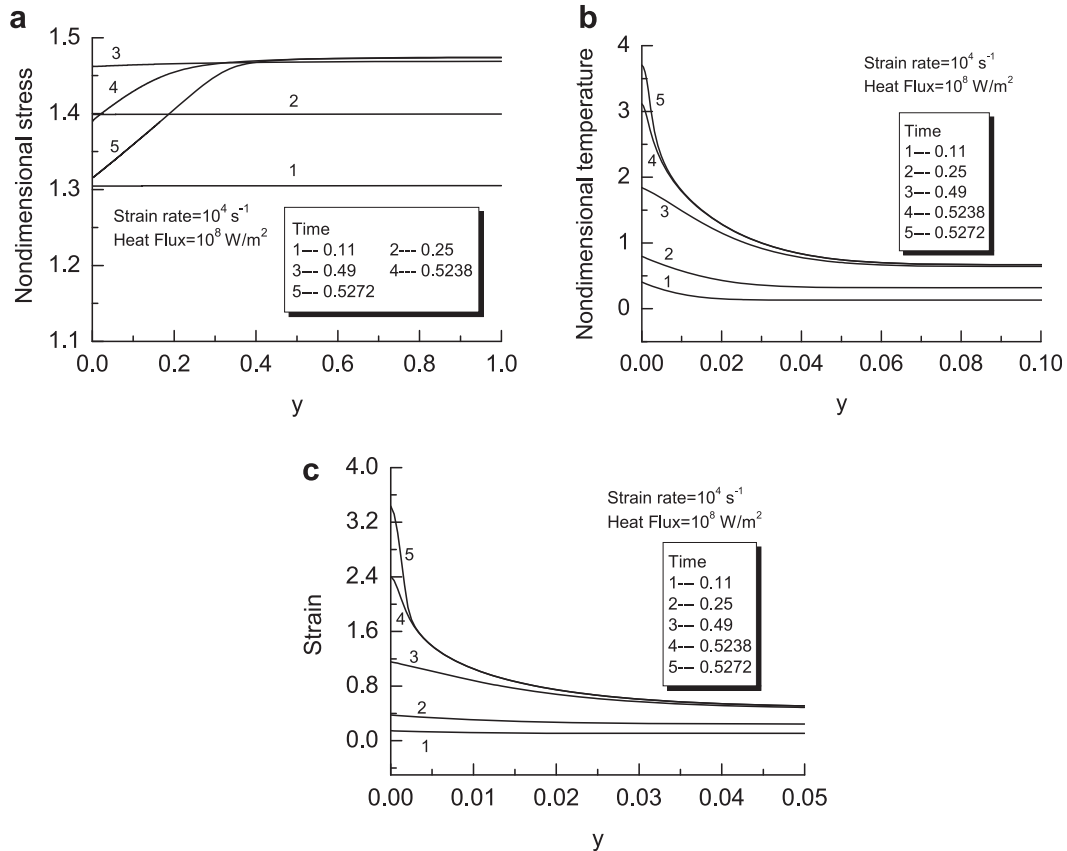


Fig. 3. For prescribed heat flux of 10^8 W/m^2 at $y = 0$ and nominal strain rate of 10^4 s^{-1} , the spatial distribution at different times of: (a) the non-dimensional shear stress, (b) the non-dimensional temperature rise and (c) the shear strain.

only very little, e.g., the temperature rise due to the interface friction heating is 338.1 K at time $0.324 \mu\text{s}$ while the total temperature rise is 360.6 K, implying that only 6% of the temperature rise is due to the plastic dissipation. For this case, the analytic solution given by Eq. (6) provides a good approximation of the temperature rise at the interface. The convex shape of the temperature rise vs. the elapsed time curve is the characteristic of the parabolic thermal phenomenon.

In Ref. [15] we examined the effect of heat flux on the initiation of localized deformation, and concluded that the prescribed heat flux acts as a defect and the shear band initiation time depends upon it. Here, it is found that the heat flux not only perturbs the

homogeneous deformation but also makes significant contribution to the temperature rise especially when the heat flux is large and the nominal strain rate is small. Even though the present model simplifies considerably the real situation encountered at the slider–rail interface, the results shed light on general trends of how heating due to surface frictional effects and that due to plastic dissipation affect the temperature rise of a material point and contribute to the localized deformation near the interface and possibly to the melting of the material there. However, since effects of phase transformation and the latent heat required to melt a material point are not included in the analysis of the problem and a conventional thermo-viscoplastic constitutive relation has been used, additional work needs to be done to simulate melting; e.g. see Ref. [25] wherein effects of phase transformation and the latent heat required for the phase transformation are considered. It is shown in Ref. [26] that the post-localization response predicted by different thermo-viscoplastic constitutive relations varies greatly even though they have been calibrated against the same test data during the pre-localization regime. In Ref. [27] the thermo-viscoplastic response of a material is modeled by a non-Newtonian fluid whose viscosity varies with the effective strain rate and the temperature; this constitutive relation considerably simplifies the analysis.

While there are no direct experimental results on the localized deformation zones, there are some indirect results with which we can compare predictions from the present mathematical model. For example, at the center of the slider surface where electrical erosion trails off rapidly and mechanical wear begins to dominate, Watt and Stefani [21] found that the thickness of the damaged region is of the order of tens of micrometers, which agrees well with the thickness

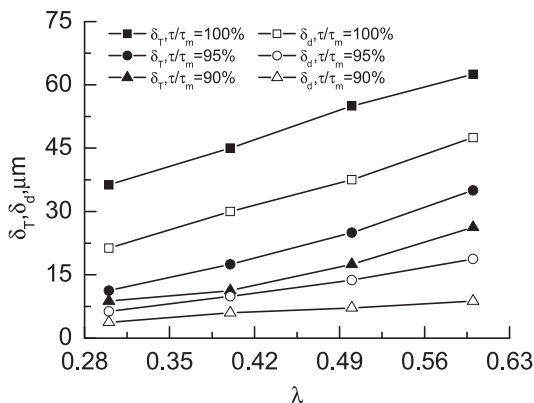


Fig. 4. At different values of the shear stress at $y = 0$, dependence of the width of the thermal and the deformation boundary layers upon the non-dimensional parameter λ .

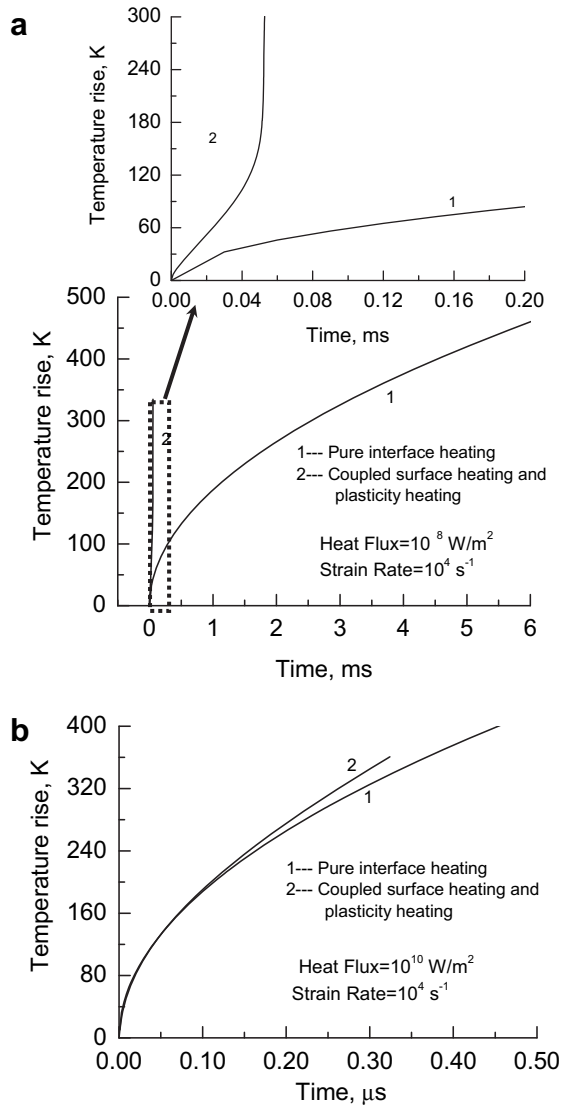


Fig. 5. The contribution of interface heating to temperature rise at $y=0$, and total temperature rise at constant heat flux and nominal strain rate for (a) heat flux = 10^8 W/m², and (b) heat flux = 10^{10} W/m².

of the region of the localized deformation predicted herein. More experimental research is needed to fully comprehend details of the deformation mechanisms prevalent at the slider–rail interface.

3. Post-melting: lubrication model

In Section 2, the temperature rise in the slider has been found. However, once the slider surface contacting the rail melts, the solid/solid contact is replaced by the liquid/solid contact. At the solid/liquid interface no-slip condition is assumed while the solid/solid contact is dominated by slipping. The liquid generated at the melt front is squeezed out from under the solid due to the pressure in the liquid film exerted by the external force. We develop below a simple lubrication theory to study the transient behavior of the molten film, such as the thickness $\delta(t)$ of the lubrication layer and the melt front velocity $V(t)$.

3.1. Formulation of the problem

We assume that a thin molten film at the sliding interface is sustained by the intense viscous dissipation, and adopt

assumptions commonly used in the lubrication theory. That is, the length of the film is assumed to be much greater than its thickness, the flow is laminar, the fluid is incompressible, the difference in the mass densities of the solid and the melt is negligible, and the bottom surface of the film is thermally insulated.

The physical system considered in this work is depicted schematically in Fig. 1(b). The leakage of the melt through the sides is ignored for simplicity, thus we model this process as a 2-D problem. The rectangular Cartesian coordinate system (x, y) is attached to the front plane of the melting material and to the horizontal plane formed by the rail surface. The momentum equation for the fluid along the x -direction is

$$\frac{dP}{dx} = \mu \frac{\partial^2 u}{\partial y^2} \quad (15)$$

Integrating Eq. (15) twice with respect to y and using the velocity boundary condition $u = 0$ at $y = \delta$, and $u = U$ at $y = 0$, we get

$$u(x, y) = \frac{1}{2\mu} \frac{dP}{dx} y(y - \delta) + U \left(1 - \frac{y}{\delta}\right) \quad (16)$$

where we have assumed that dP/dx is independent of y . The volume rate Q of the liquid flowing along the x -direction through the film is given by

$$Q = \int_0^{\delta(x)} u dy = \frac{1}{12\mu} \left(-\frac{dP}{dx}\right) \delta^3 + \frac{1}{2} U \delta \quad (17)$$

Integrating the mass conservation equation $(\partial u/\partial x) + (\partial v/\partial y) = 0$ along the y -direction using velocity boundary conditions $v = 0$ at $y = \delta$, and $v = -V$ at $y = 0$ yields

$$dQ/dx = -V \quad (18)$$

where V is the downward velocity of the armature. Combining Eqs. (17) and (18) results in a differential equation for the pressure gradient, which upon integration and using boundary conditions at the edge of the film, $P = 0$ at $x = 0$ and $x = L$, yields

$$P(x) = \frac{6\mu V}{\delta^3} x(L - x) \quad (19)$$

Integrating along the liquid film, Eq. (19) gives

$$F_n = \int_0^L P(x) dx = \mu V \left(\frac{L}{\delta}\right)^3 \quad (20)$$

The temperature distribution in the liquid film is then obtained by solving the following simplified energy equation and the adiabatic thermal condition at $y = 0$.

$$k \frac{\partial^2 T}{\partial y^2} + \mu \left(\frac{\partial u}{\partial y}\right)^2 = 0 \quad (21)$$

Combining this equation with the longitudinal velocity distribution, integrating twice with respect to y , and applying the boundary condition $T = T_m$ at $y = \delta$ and $\partial T/\partial y = 0$ at $y = 0$, we obtain [1] (note that the thickness of the melted layer is used as input to this problem):

$$T - T_m = \frac{\mu}{k} \left[\frac{G^2 \delta^4}{24\mu^2} (1 - \eta) (2\eta^3 - 2\eta^2 + \eta + 1) - \frac{G \delta^2 U}{6\mu} (1 - \eta)^2 (2\eta + 1) + \frac{U^2}{2} (1 - \eta^2) \right] \quad (22)$$

where $G(x) = -dP/dx$ and $\eta = y/\delta$.

The energy balance at the melting front requires that

$$-k \frac{\partial T}{\partial y} \Big|_{y=\delta} = \rho [h_{sf} + c(T_m - T_0)] \left(V + \frac{d\delta}{dt} \right) \tag{23}$$

where h_{sf} is the latent heat of fusion, c is the specific heat of the solid material, and T_m, T_0 are the melting and the reference temperatures of the solid body, respectively. The heat sources contribute to the latent energy required for the phase change to occur from the solid to the liquid and the energy needed to raise the temperature from T_0 to T_m . The term in the parentheses on the right-hand-side of Eq. (23) represents the unsteady melting rate and it equals the sum of the solid descending velocity and the growth rate of the film thickness.

Substituting for T from Eq. (22) into Eq. (23) we get

$$\frac{\mu}{\delta} \left[\frac{G^2 \delta^4}{12\mu^2} + U^2 \right] \approx \frac{\mu}{\delta} U^2 \tag{24}$$

For a typical molten aluminum $\delta \sim 10^{-5}$, $\mu \sim 10^{-3}$, $U \sim 10^3$, $G \sim 10^8$, we have $(G^2 \delta^4 / 12\mu^2) / (U^2) \sim 10^{-5} - 10^{-4}$, and hence one can neglect the first term in the bracket on the left hand side of Eq. (24).

In order to gain further insight into the characteristic parameters pertinent to the present system, the governing equations are non-dimensionalized. Using definitions listed in the Nomenclature, Eqs. (20), (23) and (24) can be written as

$$\bar{V} - B_e \bar{\delta}^3 = 0 \quad \left(\bar{V} + \frac{d\bar{\delta}}{d\bar{t}} \right) \bar{\delta} = \frac{S_{te\mu}}{1 + S_{te}} \tag{25}$$

where $B_e = F_n L / \mu \alpha$ is the Bejan number [3]; $S_{te} = c(T_m - T_0) / h_{sf}$ is the Stefan number and $S_{te\mu} = c\mu U^2 / kh_{sf}$ for viscous heating [3].

The steady state solution is recovered if we set $d\bar{\delta}/d\bar{t} = 0$ in Eq. (23) in which case we get

$$\bar{\delta}_S = \left[\frac{S_{te\mu}}{B_e(1 + S_{te})} \right]^{\frac{1}{4}} \quad \bar{V}_S = B_e^{\frac{1}{4}} \left(\frac{S_{te\mu}}{1 + S_{te}} \right)^{\frac{3}{4}} \tag{26}$$

In terms of dimensional variables we have

$$\delta_S = \frac{\mu^{\frac{1}{2}} U^{\frac{1}{2}} L^{\frac{3}{4}}}{\left\{ F_n \rho [h_{sf} + c(T_m - T_0)] \right\}^{\frac{1}{4}}} \tag{27}$$

$$V_S = \frac{F_n^{\frac{1}{4}} \mu^{\frac{1}{2}} U^{\frac{3}{4}}}{\left\{ \rho L [h_{sf} + c(T_m - T_0)] \right\}^{\frac{3}{4}}}$$

Eq. (27)₂ is identical to the expression derived by Stiffler [6] and has also been used in [8,9] for analyzing the armature–rail system. Similar scaling laws for the molten material thickness and melt front velocity have been obtained by Bejan [3]. For the slider melting studied here, the sensible heat $c(T_m - T_0)$ accompanying the temperature rise is either comparable to or greater than the latent heat of phase change which occurs at a constant temperature. For example, using values of parameters listed in Table 3, we have $c(T_m - T_0) / h_{sf} = 1.764$.

When the applied slider velocity U is a constant, the unsteady Eq. (25) can be simplified further by using normalized variables listed in the Nomenclature. Eqs. (25)₁ and (25)₂ reduce to

$$\hat{V} - \hat{\delta}^3 = 0 \quad \left(\hat{V} + \frac{d\hat{\delta}}{d\hat{t}} \right) \hat{\delta} = 1 \tag{28}$$

Table 3
Material parameters used in the analysis of the post-lubrication process.

$\rho = 2485 \text{ kg/m}^3$; $k = 83.7 \text{ W/(m K)}$; $c = 1084 \text{ J/(kg K)}$; $\mu = 0.0045 \text{ Pa}$;
$h_{sf} = 378000 \text{ J/(kg)}$; $T_m = 908 \text{ K}$; $T_0 = 293 \text{ K}$; $L = 0.0155 \text{ m}$

and eliminating \hat{V} from Eq. (28) gives the following simple first-order differential equation for $\hat{\delta}$.

$$\frac{d\hat{\delta}^2}{d\hat{t}} = 2 \left(1 - \hat{\delta}^4 \right) \tag{29}$$

Solving Eqs. (28) and (29) with the initial condition $\hat{\delta}(0) = 0$ results in

$$\hat{\delta}(\hat{t}) = \tanh^{\frac{1}{2}}(2\hat{t}) \quad \hat{V}(\hat{t}) = \tanh^{\frac{3}{2}}(2\hat{t}) \tag{30}$$

Eq. (30) is the same as that derived in Ref. [13] for the solution of the unsteady problem describing gravity-induced melting on a flat plate. It is found that, in contrast with the results for the steady state problem, both the thickness and the velocity increase first rapidly from zero, and after a certain time period, both approach the steady state value of 1. If we chose $\hat{\delta}_C = 0.99$ as the criterion for the steady state to have reached then the corresponding time $\hat{t}_C = 1.15$. For $P = 75 \text{ MPa}$ and $U = 1000 \text{ m/s}$, $t_C = 0.58 \text{ ms}$ and $D_C = 0.58 \text{ m}$ for $\hat{\delta}_C = 0.99$. We note that the length of the rail used in experiments is about 2 m [12], and *this strongly suggests the importance of incorporating transient effects in the description of the dynamics of an armature–rail system.* Furthermore, since the velocity is assumed to be constant, the dimensional critical time and distance can be written as

$$t_C = \frac{Z}{P^{1/2} U}, \quad D_C = U t_C = \frac{Z}{P^{1/2}} \tag{31}$$

where $Z = (1/4) \ln((1 + \hat{\delta}_C^2) / (1 - \hat{\delta}_C^2)) (L^3) / (\alpha) \{ \rho [h_{sf} + c(T_m - T_0)] \}^{1/2}$. It is interesting to note that once the normalized critical thickness $\hat{\delta}_C$ has been chosen, the distance D_C is independent of the velocity U while t_C is a decreasing function of U . Both t_C and D_C are inversely proportional to $P^{1/2}$ and are independent of the viscosity μ .

In many applications, such as electromagnetic launching, the speed of armature varies with time. In this case, there is no general analytic solution of Eq. (25). Thus we rewrite Eq. (25)₂ as

$$\frac{d\bar{\delta}^2}{d\bar{t}} = 2 \left[W \bar{U}^2(\bar{t}) - B_e \bar{\delta}^4 \right] \tag{32}$$

where $W = ((C\mu\alpha^2) / (kh_{sf}L^2(1 + S_{te})))$ is a new non-dimensional quantity. Eq. (32) can be numerically solved provided that $U(-t)$ is known. Here we use the fourth order Runge–Kutta method [22] to solve this equation with $\bar{\delta}(0) = 0$. An important feature of our model is its ability to predict the transient response that occurs during high speed sliding, such as the armature launch process.

3.2. Comparison with experimental results

The melting and the loss of aluminum armature in a rail gun system is a common phenomenon that has been confirmed by a thin layer of aluminum deposited on the copper rail surface [7]. The following two mechanisms of this melting have been postulated: skin effect due to the Joule heating and wear mechanisms due to viscous heating [23]. Using tungsten pins embedded in the surface of an armature Stefani and Parker [12] experimentally showed that both mechanisms are important in wearing out armatures. They also measured purely mechanical (frictional and viscous) wear when the sliders were electrically insulated from the driving current. They thus showed that the viscous heating is the dominant wear mechanism at high velocities ($>1000 \text{ m/s}$). Kothmann and Stefani [8] studied the lubrication of molten film using Stiffler’s model [6]. Subsequently Merrill and Stefani [9] included the effect of turbulence in their model. However, in both models the agreement between the predictions and the

experimental results is only satisfactory. Despite these efforts, details of the liquid film formation are not yet fully understood. Here we compare the experimental data with predictions from the present model for the transient problem.

Fig. 6 shows Stefani and Parker's [12] experimentally obtained relation between the melt front velocity and the slider velocity for purely mechanical heating. These data confirm that there is a threshold velocity, around 800 m/s, for the onset of a liquid film. Below this threshold velocity the interface is believed to be solid-on-solid contact, and above this threshold velocity a layer of liquid aluminum replaces the solid-on-solid contact. As discussed above, transient effects may be important in these cases, especially during the initial liquid film formation process. Thus the solution of the transient problem provides an improved interpretation of the experimental phenomenon and uncovers new physics that the solution of the steady state problem does not provide. From results exhibited in Fig. 6 we estimate threshold velocities to be 800, 975, 775, 800 and 650 m/s, respectively, for pressure equal to 45, 75, 89, 117 and 150 MPa.

To reveal a possible scaling law like that appearing in Eq. (28), we plot on a log–log scale computed values of physical parameters such as the slider velocity, the thickness and the melt velocity. We assume that $U = at$ with $a = 10^6 \text{ m/s}^2$ [12] and $\delta(0) = \delta(0) = 0$ at the threshold velocity. Values of material and geometric parameters, loads and the approximate threshold velocity, taken from Ref. [12], are listed in Table 3. Results plotted in Fig. 7 show that the thickness of molten film grows rapidly after reaching the threshold velocity, and shortly afterwards the curves correspond to the solution of the steady state problem and obey the scaling law $\delta \sim U^{1/2}$ as predicted by Eq. (27)₁.

The predicted relations between the melt front velocity and the slider velocity, and between the melt front velocity and the applied pressure on a log–log plot are exhibited in Fig. 8(a), (b) along with the experimental data. As for the results shown in Fig. 7, we conclude from the results plotted in Fig. 8 that the melt front velocity grows dramatically first when the slider velocity reaches the threshold velocity and subsequently it approaches the steady state value obeying the scaling law $V \sim U^{3/2}$ as given by Eq. (27)₂. The experimental data are consistently higher than the model predictions with differences between the two sets of data being smaller during the transient deformations than those during the steady state deformations. However, the two sets of data agree qualitatively with each other. The experimental data near the threshold velocity is not currently available.

Results displayed in Fig. 8(b) reveal that experimental values of the pressure are consistently higher than those obtained from the

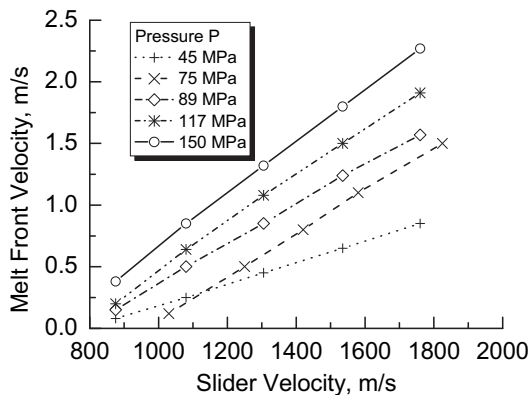


Fig. 6. Experimental results showing the relation between the melt front velocity and the slider velocity for purely mechanical heating.

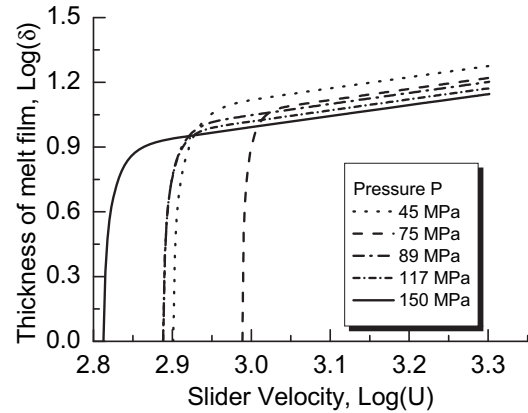


Fig. 7. On a log–log plot, variation of the thickness of the melt film with the slider velocity using the solution of the transient problem.

solution of the transient problem. The slope of each one of these curves computed by using linear regression fit to the test data equals about 1. However, the slope of a straight line fitted to values obtained from the solution of the transient problem is 0.25 indicating the existence of the scaling relation $V = P^{1/4}$, which is the same as the solution listed in Eq. (27)₂ of the steady state problem. One exception is that the slope of the straight line passing through the predicted values at pressure ranging between 45 MPa and 89 MPa and at the slider velocity of 875 m/s equals 0.76 (this is due to transients effects), which is close to that observed experimentally.

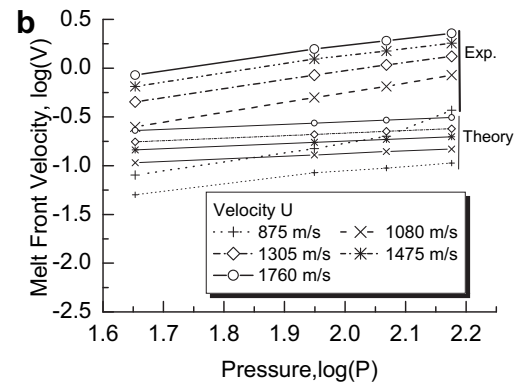
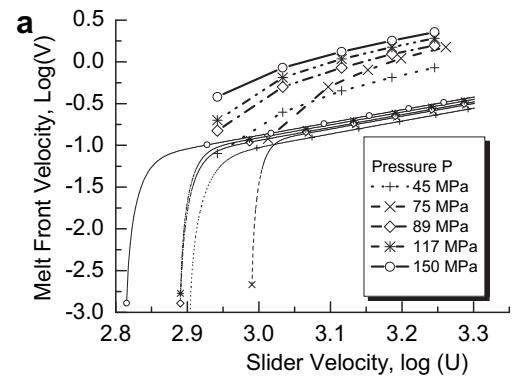


Fig. 8. On a log–log plot, the variation of (a) the melt front velocity and the slider velocity; (b) the melt front velocity with the applied pressure using the solution of the transient problem and comparison with the experimental data.

The mathematical model for the transient problem describes well the scaling law between the melt front velocity and the slider velocity but it only provides a partial interpretation of the melt front velocity–pressure relation; possible reasons for this are still unknown. We note that effects such as resolidification and turbulence have been considered in Ref. [8,9]. Another possible contributor may be the elastoviscoplastic behavior of solid materials as mentioned in Ref. [9]. At higher pressures, the contribution of material strength may play an important role.

In summary, this paper provides a simple model of the contact-melting process. However, the melting and the lubrication processes in a real armature–rail are quite complex. A complete description of the rich phenomena encountered at high speed sliding such as electromagnetic launching, Lorentz force, Joule heating, chemical reactions, and electro-migration should be considered. Furthermore, the governing equations used here include the simplified lubrication equation in which the inertia and convective effects are ignored. This simplification of the complete transient governing equations is appropriate for use in conventional tribology but its applicability needs to be examined in more detail for the high speed sliding.

4. Conclusions

We have provided a simple model for the analysis of the solid/solid contact, solid/liquid contact melting and subsequent coating of the rail by a liquid film, and have found the melt time and the corresponding distance traveled by the slider by assuming that the temperature rise is due to high speed interface friction and heat conduction. Simple scaling laws for both the melting time and the corresponding distance traveled have been derived when either the slider velocity or its acceleration is constant. These estimates have been refined by also considering the energy dissipated due to plastic deformations of the slider, and solving the resulting coupled thermo-mechanical problem by the finite element method. It is found that two boundary layers – one encompassing high strains and the other elevated temperatures – form near the slider–rail interface. The thickness of the thermal boundary layer is generally larger than that of the deformation boundary layer, and both are of the order of 10 μm . The boundary layer is likely a precursor to the formation of the molten film in the coupled thermo-mechanical system. Large values of the heat flux at the slider–rail interface generated due to high speed friction contribute more to the temperature rise than the energy dissipated due to plastic working.

The analysis of the steady state problem based on the lubrication theory provides only a first-order approximation of the melting process. However, as illustrated in the paper, the solution of the transient problem reveals that it is hard to achieve the steady state in a real system. The experimental data collected in a process dominated by purely mechanical heating can be described well by the solution of the transient problem, especially the scaling law of velocity dependence. The solution of the transient problem can only partially address the experimentally observed dependence of the slider velocity upon the pressure. Thus other mechanisms which are sensitive to the applied pressure such as the shear strength of a solid material near its melting temperature ought to be included in the model.

Acknowledgments

Z. Wei would like to thank Drs. Ganesan and Ravi-Chandar of the University of Texas–Austin for their support and help during this research. Z. Wei's work was partially supported by the Office of Naval Research (ONR) MURI Grant # N00014-04-1-0599 RQ–M awarded to the University of Texas–Austin. RCB's work was partially funded by the ONR grant N00014-06-1-0567 awarded to Virginia Polytechnic Institute and State University.

References

- [1] Bejan A. The fundamentals of sliding contact melting and friction. *J Heat Transfer* 1989;111:13–20.
- [2] Bejan A. Contact melting heat transfer and lubrication. *Adv Heat Transfer* 1994;24:1–38.
- [3] Bejan A. *Convection heat transfer*. 3rd ed. John Wiley & Sons, Inc.; 2004. p. 478–90.
- [4] Bejan A. Contact melting during sliding on ice. *Int J Heat Mass Transfer* 1993;36:1171–9.
- [5] Montgomery RS. Friction and wear at high sliding speeds. *Wear* 1976;36:275–98.
- [6] Stiffler AK. Friction and wear with a fully melting surface. *J Tribol* 1984;106:416–9.
- [7] Persad C, Yeoh A, Prabhu G, Write G, Eliezer Z. On the nature of the armature–rail interface: liquid metal effects. *IEEE Trans Magn* 1997;33:140–5.
- [8] Kothmann RE, Stefani F. A thermal hydraulic model of melt-lubrication in rail gun armatures. *IEEE Trans Magn* 2001;35:86–91.
- [9] Merrill R, Stefani F. A turbulent melt-lubrication model of surface wear in rail gun armatures. *IEEE Trans Magn* 2005;41:414–9.
- [10] Liou NS, Okada M, Prakash V. Formation of molten metal films during metal-on-metal slip under extreme interfacial conditions. *J Mech Phys Solids* 2004;52:2025–56.
- [11] Bowden FP, Tabor D. *The friction and lubrication of solids*. Oxford University Press; 2001.
- [12] Stefani F, Parker JV. Experiments to measure wear in aluminum armatures. *IEEE Trans Magn* 1999;35:100–6.
- [13] Yoo H. Analytical solutions to the unsteady close-contact melting on a flat plate. *Int J Heat Mass Transfer* 2000;43:1457–67.
- [14] Yoo H. Initial transient behavior during close-contact melting induced by convective heating. *Int J Heat Mass Transfer* 2001;44:2193–7.
- [15] Batra RC, Wei ZG. Shear bands due to heat flux prescribed at boundaries. *Int J Plast* 2006;22:1–15.
- [16] Batra RC, Kim CH. Analysis of shear banding in twelve materials. *Int J Plast* 1992;8:425–52.
- [17] Carslaw HS, Jaeger JC. *Conduction of heat in solids*. Oxford; 1986.
- [18] Ghassemi M, Barsi YM. Effect of liquid film (Indium) on thermal and electromagnetic distribution of an electromagnetic launcher with new armature. *IEEE Trans Magn* 2005;41:408–13.
- [19] Johnson GR, Cook WH. A constitutive model and data for metals subjected to large strain rates and high temperatures. In: *Proceedings of the seventh international symposium on ballistics*, The Hague, The Netherlands; 1983. p. 541–48.
- [20] Cho KM, Lee S, Nutt SR, Duffy J. Adiabatic shear band formation during dynamic torsional deformation of HY-100 steel. *Acta Metall Mater* 1993;41:923–32.
- [21] Watt T, Stefani F. The effect of current and speed on perimeter erosion in recovered armatures. *IEEE Trans Magn* 2005;41:448–52.
- [22] Hoffman JD. *Numerical methods for engineers and scientists*. 2nd ed. New York: Marcel Dekker, Inc.; 2001.
- [23] Baber JP, Bauer DP, Jamison K, Parker JV, Stefani F, Zielinski A. A survey of armature transition mechanism. *IEEE Trans Magn* 2003;39:47–51.
- [24] Batra RC, Chen L. Effect of viscoplastic relations on the instability strain, shear band initiation strain, the strain corresponding to the minimum shear band spacing, and the band width in a thermoviscoplastic materials. *Int J Plast* 2001;17:1465–89.
- [25] Zhu ZG, Batra RC. Consideration of phase transformations in the study of shear bands in a dynamically loaded steel block. *J Eng Mater Tech* 1992;114:368–77.
- [26] Batra RC, Kim CH. Effect of viscoplastic flow rules on the initiation and growth of shear bands at high strain rates. *J Mech Phys Solids* 1990;38:859–74.
- [27] Batra RC, Liu DS. Adiabatic shear banding in plane strain problems. *J Appl Mech – Trans ASME* 1989;56:527–34.